Interfacial acidity on oxide surfaces: A scaling paradigm and the role of the hydrogen bond

Robert C. Chapleski, Jr.,[†] Azhad U. Chowdhury,[§] K. Reid Mason,[†] Robert L. Sacci,[§] Benjamin Doughty,[*,§] and Sharani Roy[*,†]

† Department of Chemistry, University of Tennessee, Knoxville, TN 37996, USA

§ Chemical Sciences Division, Oak Ridge National Laboratory, Oak Ridge, TN 37831, USA

E-mail: sharani.roy@utk.edu

E-mail: doughtybl@ornl.gov

Abstract

A fundamental understanding of acidity at an interface, as mediated by structure and molecule-surface interactions, is essential to elucidate the mechanisms of a range of chemical transformations. While the strength of an acid in the gas and solution phases is conceptually well understood, how acid-base chemistry works at an interface is notoriously more complicated. Using density functional theory and nonlinear vibrational spectroscopy, we have developed a method to determine the interfacial Brønsted-Lowry acidity of aliphatic alcohols adsorbed on the {100} surface of the model perovskite, strontium titanate. Here we show that, while shorter and less branched alkanols are less acidic as a gas and more acidic in solution, shorter alcohols are less acidic whereas less substituted alkanols are more acidic at the gas-surface interface. Hydrogen bonding plays a critical role in defining acidity, whereas structure-acidity relationships are dominated by van der Waals interactions between the alcohol and the surface.

The Brønsted-Lowry strength of an acid in a homogeneous gas or solution is defined by how readily it donates a proton. In a heterogeneous environment, however, where the separation between a donated proton and its conjugate base is determined by the chemical asymmetry of the interface, hydrogen bonding, and molecular ordering, characterizing acidity becomes nebulous. In fact, there is a long-standing controversy regarding the basicity of an air-water interface, where a confluence of experimental and theoretical work shows conflicting results and interpretations.[1, 2] A major limitation in these measurements is that the gas-liquid interface is dynamic and remarkably sensitive

to trace impurities that alter the surface chemical composition. The gas-solid interface, while more rigid than the gas-liquid interface, complicates the picture of acidity by adsorbing molecules at specific sites and tuning their proton transfer via gas-surface interactions. In this scenario, molecular acidity is not determined by the properties of the molecule or the surface independently, but rather by chemical subtleties of adsorption and interfacial proton dissociation. This complexity motivates us to develop a paradigm of gas-solid interfacial acidity that advances the fundamental description of acid strength beyond that found in homogeneous gaseous and solution environments. Such a paradigm can be highly beneficial to elucidate acid-base reactivity at a range of interfaces.

Perovskites, a broad class of oxide materials, have shown promise in the synthesis of materials ranging from biofuels to pharmaceuticals via heterogeneous acid-base catalysis. To date, several studies have pursued a fundamental understanding of the acid-base character of the *surface* in catalytic reaction mechanisms,[3-11] wherein the acidic or basic nature of metal-oxide surface sites was investigated by monitoring the products of a small probe alcohol, such as isopropanol, reacting at the surface of strontium titanate ($SrTiO_3$, henceforth abbreviated as STO): at an acidic site, a single isopropanol molecule can undergo dehydration to form propylene and water, while at a basic site, acetone and H_2 are formed via dehydrogenation.[7, 12-18] However, an opposite trend was found for ethanol; Foo et. al. recently found that the rate of ethanol dehydrogenation increases with the ratio of acidic sites on multifaceted STO nanocubes.[5] This apparent contradiction emphasizes the need to understand the acidity

of alkanols at an oxide surface and clarify the mechanisms that control it at the molecular level.

We report the interfacial acidity of a family of small alkanols adsorbed to a well-defined and atomically flat STO{100} surface using a combination of density functional theory (DFT) and vibrational sum-frequency generation (SFG) methods. SFG experiments selectively probe interfacial molecular species and provide vibrational spectra that are compared with DFT results.[17, 19] Using this combined DFT+SFG approach, we describe the mechanisms of adsorption and proton transfer in terms of the interactions of aliphatic alcohols with the oxide surface, with a focus on the structure of the alkanol. To this end, we are able to bridge previous theoretical investigations of alkanol adsorption on STO{100},[7] revealing the essential role of hydrogen bonding on the adsorption equilibria. Finally, we describe the interfacial acidity of the series of aliphatic alcohols from methanol to butanol on STO{100} using partition functions constructed from DFT calculations, and compare the structure-acidity relationships to the known, corresponding relationships in the gas phase and in aqueous solution.

Our investigation commences with a study of the adsorption of isopropanol on the TiO_2-terminated surface of STO{100}. In the first section, we compute the pathway for isopropanol adsorption, leading to a description of a two-state equilibrium on the surface. We then implement SFG not only to experimentally verify the presence of this two-state chemisorption equilibrium for isopropanol, but also to reveal similar equilibria for other alkanols on STO{100}, with characteristic spectral shifts related to hydrogen-

bonding interactions. We conclude by applying these two-state equilibria to calculate the interfacial Brønsted-Lowry acid strengths of alkanols and determine the structural and chemical factors that control the acidity.

Results and Discussion

DFT results for adsorption of isopropanol in four different molecular orientations at the most favorable binding site (Ti-atom top site) on the TiO_2-terminated STO{100} surface are shown in Fig. 1. Based on calculated surface and adsorption energies, we find that the TiO_2-termination is energetically more stable than the SrO-termination and thus consider the former exclusively in this work (see Supplementary Section I.A.). The preferred binding site was determined from a two-dimensional adsorption-energy scan along the surface plane (see Supplementary Section I.B.). The four orientational minima were obtained via out-of-plane molecular rotation about the C-O bond. A comparison of energies of the four orientations shows that strong adsorption arises from binding of the Ti atom to the O_{alk} atom, as seen in the "α-H close" (α-hydrogen pointing towards the surface, E_{ads} = 1.25 eV), "CH_3 away" (one of the methyl groups pointing away from the surface, E_{ads} = 1.25 eV), and "α-H away" (α-hydrogen pointing away from the surface, E_{ads} = 1.22 eV) cases ("*surf*" = surface, "*alk*" = alkoxy, positive adsorption energies (E_{ads}) indicate favorable adsorption). When the O_{alk} atom is pointed away from the surface and does not interact with Ti, as in the "OH away" orientation, adsorption is considerably weakened (E_{ads} = 0.42 eV). Notably, the adsorption of isopropanol in any of the four orientations does not cause significant distortion of the surface structure.

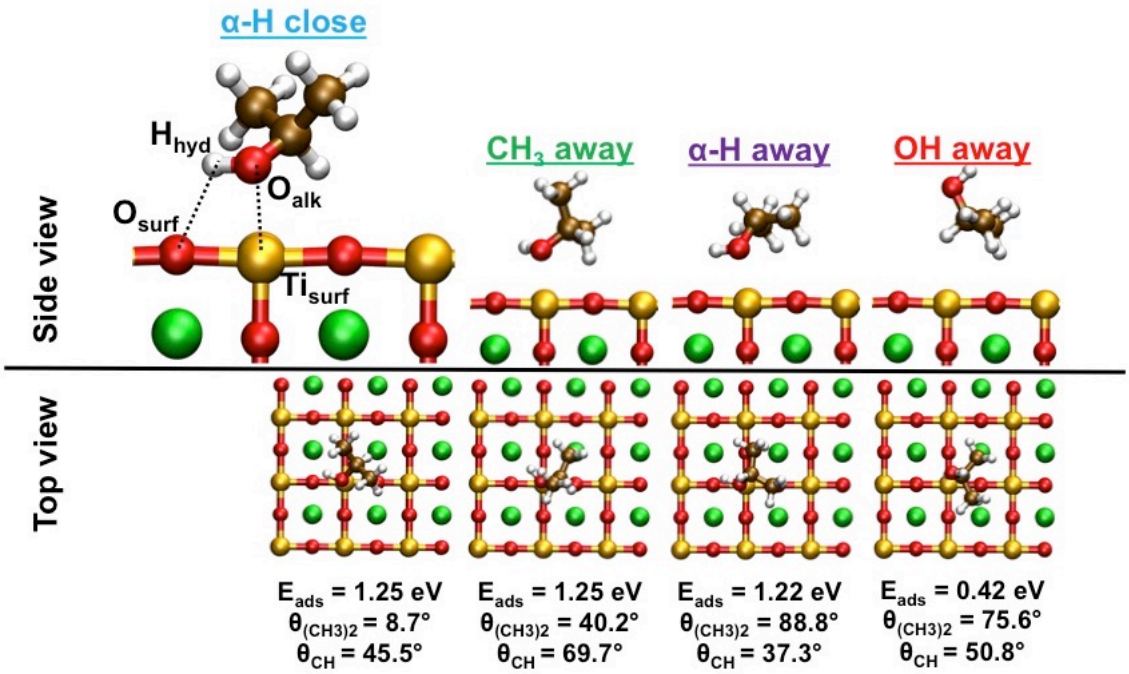

Fig. 1: Side- and top-views of optimized geometries of four different molecular orientations of isopropanol adsorbed on STO{100}, calculated using DFT. Below each structure, adsorption energies and orientation angles $\theta_{(CH3)2}$ and θ_{CH} are provided, as described in the text. For "α-H close," dashed lines illustrate bonds that will be formed in subsequent adsorption steps. Color scheme: Sr: green, Ti: yellow, O: red, C: brown, H: white.

DFT results for dissociative adsorption of isopropanol following transfer of the hydroxyl proton (H_{hyd}) from adsorbed molecular isopropanol to the neighboring O_{surf} atom for the "α-H close," "CH_3 away", and "α-H away" orientations are shown in Fig. 2. Because such a proton transfer is highly unlikely in the "OH away" orientation, it was not included in the remainder of our study. For each of the remaining orientations, our computations reveal that proton transfer results in the formation of two adsorption states that differ from each other in a subtle but important way. In the first state, with structures shown in

Fig. 2a, we find that, while H_{hyd} has transferred to the O_{surf} atom, a hydrogen bond remains between this proton and the O_{alk} atom; therefore, the proton has not fully dissociated from the isopropoxide species. The second state, in contrast, results from complete dissociation of H_{hyd} from O_{alk} upon subsequent breakage of the hydrogen bond, as shown in Fig. 2b. The adsorption energies of the hydrogen-bonded forms are E_{ads}("α-H close") = 1.40 eV, E_{ads}("CH_3 away") = 1.34 eV, and E_{ads}("α-H away") = 1.38 eV, whereas the adsorption energies of the non-hydrogen-bonded forms are E_{ads}("α-H close") = 1.43 eV, E_{ads}("CH_3 away") = 1.48 eV, and E_{ads}("α-H away") = 1.48 eV. A comparison of adsorption energies in Figs. 1 and 2 shows that dissociative chemisorption of isopropanol is stronger than non-dissociative, molecular physisorption of isopropanol for all molecular orientations, and the second chemisorbed form with no hydrogen bond is adsorbed more strongly than the hydrogen-bonded form. Supplementary Tables S1-S3 show the bond lengths and angles involving the Ti, O_{surf}, O_{alk}, and H_{hyd} atoms in the physisorbed and chemisorbed forms of isopropanol. Notably, when the hydrogen bond breaks, the angle between the O_{surf}-H_{hyd} bond and the surface normal changes from 14-17° in Fig. 2a to 64-66° in Fig. 2b, indicating that the hydrogen atom moves closer to the TiO_2-surface plane to increase interactions with other nearby O_{surf} atoms. This large change in the orientation of the O_{surf}-H_{hyd} bond might have important effects on the subsequent reaction pathways of isopropanol.

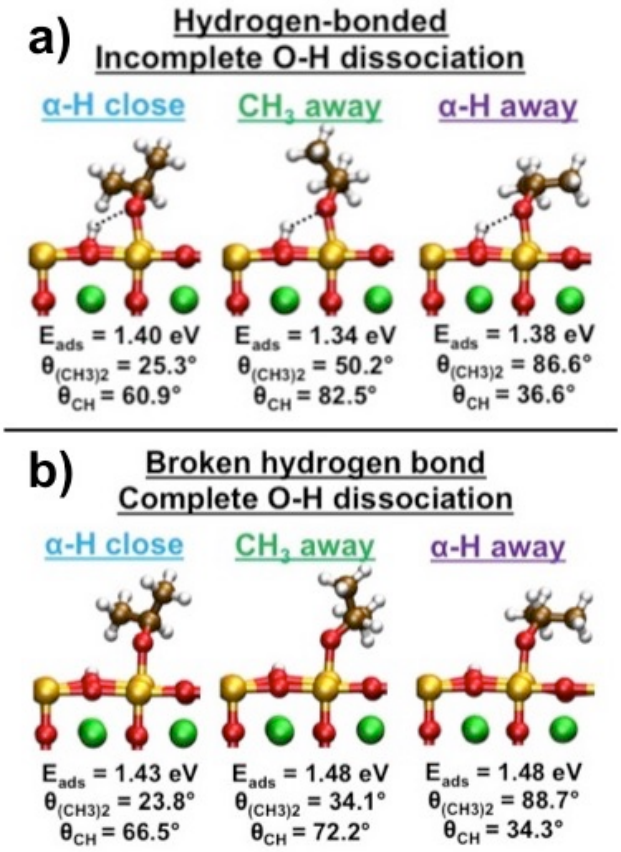

Fig. 2: Side views of optimized geometries of three different orientations of isopropanol on STO{100} following proton transfer, calculated using DFT. Below each structure, its adsorption energy and orientation angles are noted. Structures in (a) exhibit a hydrogen bond (dashed line) between the H_{hyd} and O_{alk} atoms, and structures in (b) result from the disruption of this hydrogen bond. Same color scheme as in Figure 1.

DFT-computed energy pathways for adsorption followed by proton transfer for three orientations ("α-H-close," "CH_3-away", and "α-H-away") of isopropanol on STO{100} are shown in Fig. 3. The calculated activation energy for proton transfer (dissociative chemisorption) is 0.24 ± 0.04 eV over three orientations, and the calculated activation

energy for subsequent hydrogen-bond-dissociation is 0.02 eV ± 0.02 eV over three orientations. The calculated value of 0.24 eV for proton transfer is similar to that found in the literature.[7] Zero-point corrections reduce the activation energy for proton transfer to 0.12 ± 0.05 eV and negligibly change the activation energy for hydrogen-bond dissociation. The low values of activation energies suggest that adsorbed isopropanol exists in a thermal equilibrium between the molecular and dissociated forms. A Boltzmann population analysis shows that at 298 K, 0.01% of the adsorbed isopropanol exists in the molecular form, 3.00% exists in the deprotonated and hydrogen-bonded form and 96.98% exists in the deprotonated and non-hydrogen-bonded form. Predictably, an increase in temperature increases the relative population of the hydrogen-bonded form. At 500 K, relevant to the catalytic transformations of isopropanol,[7, 17, 18] 0.46% of the adsorbed isopropanol exists in the molecular form, 10.98% exists in the deprotonated and hydrogen-bonded form and 88.57% exists in the deprotonated and non-hydrogen-bonded form.

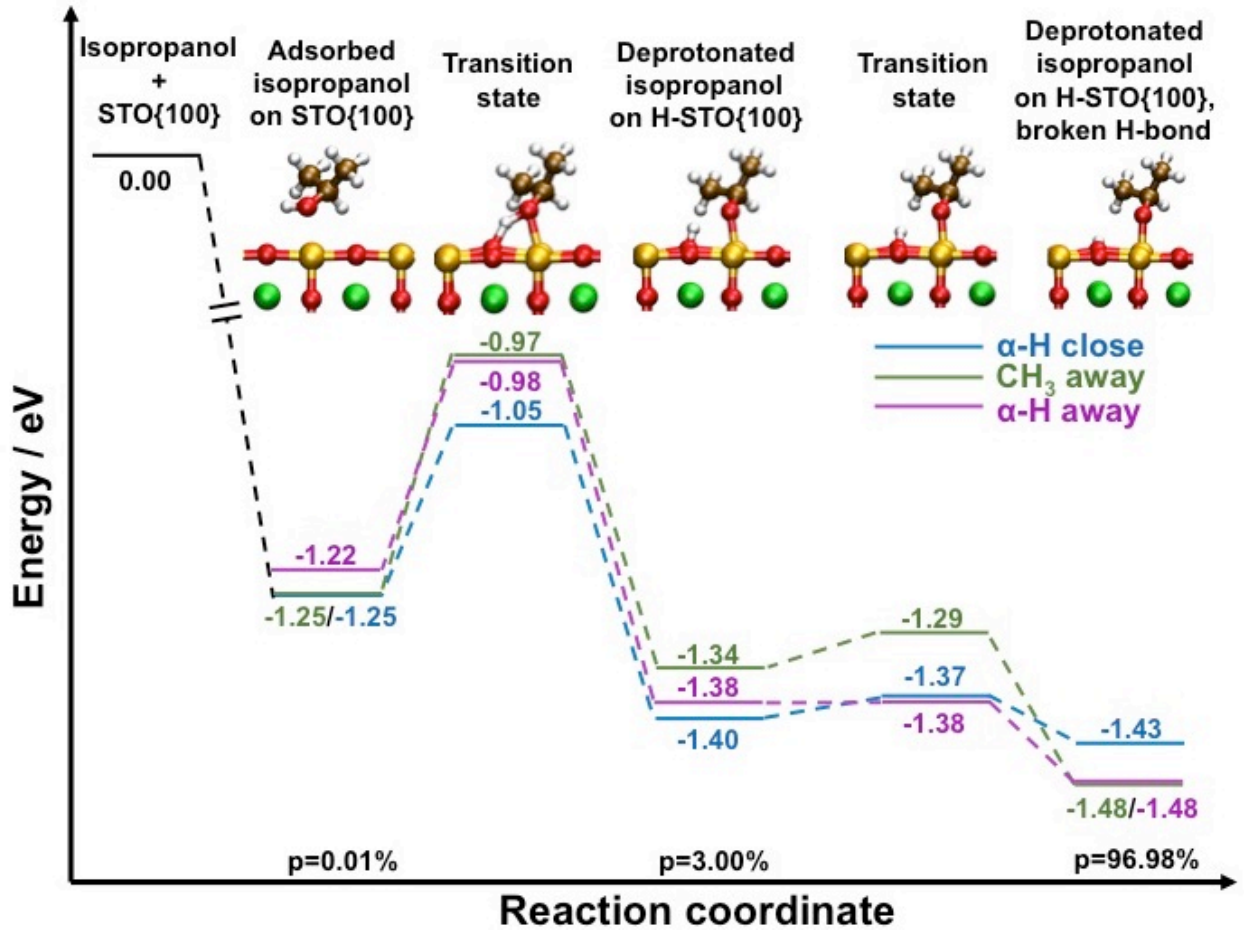

Fig. 3: Energy pathway of adsorption and proton transfer of isopropanol on STO{100} calculated using DFT for all molecular orientations shown in Figures 1 and 2. *p* values are sums of Boltzmann populations of all orientations for a given species at 298 K. Insets show geometries of stationary points along the "α-H close" pathway. Same color scheme as in Figure 1.

Previous work by Doughty and coworkers examined the C-H stretching region of isopropanol adsorbed on STO{100} at 298 K and mapped the absolute orientation of adsorbed isopropanol using SFG methods. One of the orientational angles bisects the CH_3-C-CH_3 angle in isopropanol to form an angle, $\theta_{(CH3)2}$, of 29 ± 7° with respect to the

surface normal, and another, along the α-C-H bond, formed an angle, θ_{CH}, of 51 ± 8°.[17] These measured angles strongly agree with the corresponding calculated angles of the deprotonated forms of isopropanol in the "α-H close" orientation (Fig. 2). This result also corroborates our theoretical results using Boltzmann population analysis (*vide supra*) that the adsorption equilibrium largely favors the chemisorbed over the physisorbed form of isopropanol.

To search for the existence of our DFT-predicted chemisorbed forms of alcohols on STO{100}, we measured the SFG spectra in the O-H stretching region for methanol, ethanol, isopropanol, and sec-butanol in the SSP polarization combination, with results plotted in Figure 4. The spectrum of each alcohol adsorbed on STO{100} shows a narrow, intense band at around 3640 cm^{-1} and a broad, lower-intensity band at around 3550-3600 cm^{-1}. Based on a normal-mode analysis of the dissociatively chemisorbed forms of the four alcohols, as shown in Table 1, the broad, lower-frequency band is assigned to the O_{surf}-H_{hyd} stretch when H_{hyd} is hydrogen-bonded to the adsorbed alkoxide, and the narrow, higher-frequency band is assigned to the "free" O_{surf}-H_{hyd} stretch wherein the hydrogen bond is disrupted. This experimental result with computationally aided assignment directly supports a two-state chemisorption equilibrium. Due to the low Boltzmann population of the physisorbed form of the alcohol, the O_{alk}-H_{hyd} stretch does not appear in the spectrum.

Both DFT and SFG results find very little variation in the O_{surf}-H_{hyd} stretching frequency for the broken-hydrogen-bond species across the four alcohols. In the SFG spectra,

these frequencies for ethanol, isopropanol, and sec-butanol were nearly identical, and DFT finds a range of only 12 cm^{-1} over corresponding values. More importantly, however, the O_{surf}-H_{hyd} frequencies for the hydrogen-bonded species in the SFG spectra vary over the four alcohols and parallel the frequencies predicted by DFT, with sec-butanol > methanol > isopropanol > ethanol. The red shift in the O_{surf}-H_{hyd} stretch arises from the increase in the strength of the hydrogen bond, as corroborated by a variation in the lengths of the hydrogen bond (i.e., O_{alk}-H_{hyd} distance): 1.95 Å (sec-butanol) > 1.91 Å (methanol) > 1.90 Å (isopropanol) > 1.88 Å (ethanol). This agreement between DFT and SFG reinforces our assignment of the broad band in this region to the O_{surf}-H_{hyd} stretch in the hydrogen-bonded state and suggests that trace amounts of water are not responsible for the measured spectral features. The strength of the hydrogen bond is determined by the competition between the amount of electron density on the alkoxide oxygen and the extent of weakening of alkoxide-surface interactions due to geometric strain from the hydrogen bond. A similar trend is seen for the frequency of the O_{surf}-H_{hyd} wagging mode (see Supplementary Table S4), which red-shifts with decreasing strengths of the associated hydrogen bond.

Along with frequencies, ranges for isopropanol O_{surf}-H_{hyd} stretching frequencies derived from DFT results are provided in Table 1. Spectral widths also show agreement between DFT and SFG values. For DFT results, the quoted widths are reported as average absolute deviations from the mean of three frequencies, corresponding to the three orientations shown for each of the two states in Figure 2 (see Supplementary Table S5). Both DFT and SFG affirm that the hydrogen-bonded state results in a

broader spectral feature in comparison to the broken-hydrogen-bond state. Notably, a larger sampling of out-of-plane orientations is afforded in the more freely rotating hydrogen-bonded alkoxide compared to the broken-hydrogen-bond state due to a closer O_{alk}-Ti_{surf} distance in the latter form (*vide infra*). This enhanced orientational freedom results in a broader O_{surf}-H_{hyd} spectral feature for the hydrogen-bonded species observed in both experiment and theory.

Table 1: Unscaled O_{surf}-H_{hyd} stretching frequencies for hydrogen-bonded and broken-hydrogen-bond species of selected alkanols on STO{100}, obtained from SFG and DFT. For isopropanol DFT frequencies, the mean frequency and average absolute deviation from the mean computed over three orientations (Fig. 2) are presented. Peak widths are provided for all SFG spectral features. All units are in cm^{-1}.

	O_{surf}-H_{hyd} stretch, hydrogen bonding (**DFT**)	O_{surf}-H_{hyd} stretch, hydrogen bonding (frequency / width) (**SFG**)	O_{surf}-H_{hyd} stretch, broken-hydrogen-bond (**DFT**)	O_{surf}-H_{hyd} stretch, broken-hydrogen-bond (frequency / width) (**SFG**)
methanol	3383	3568 / 40	3580	3645 / 6
ethanol	3331	3548 / 24	3586	3641 / 6
isopropanol	3363 $\pm$ 28	3567 / 34	3581 $\pm$ 1	3641 / 6
sec-butanol	3440	3570 / 26	3592	3641 / 6

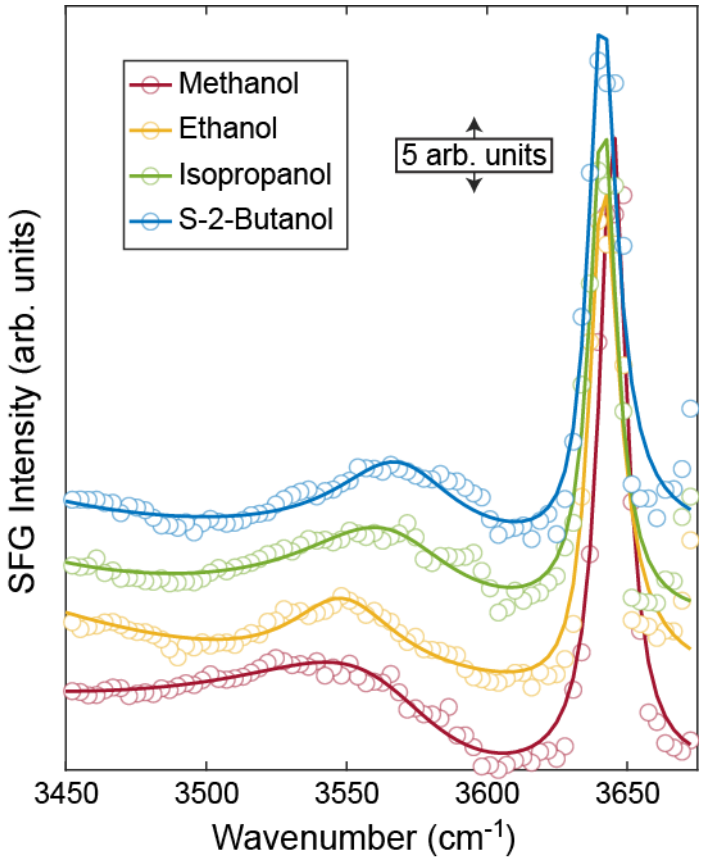

Fig. 4: SFG spectra of methanol, ethanol, isopropanol, and sec-butanol (S-2-butanol) adsorbed onto STO{100} in the SSP polarization combination. Traces are offset vertically for clarity.

The Brønsted-Lowry acidity ($HA \rightleftharpoons H^+ + A^-$) of an aliphatic alcohol is dictated by the polarizability of the alkyl moiety in the gas phase and solvation of the alcohol in the solution phase. In the gas phase, alkyl substituents on the α-carbon and longer alkyl chains help to polarize the electron cloud on the alkyl moiety in a direction that stabilizes the negative charge on the alkoxide conjugate base. Consequently, the gas-phase acidity increases as: methanol < ethanol < n-propanol < n-butanol < isopropanol < tert-butanol.[20-24] However, in aqueous solution, alkyl substituents on the α-carbon and

longer alkyl chains weaken solvation of the conjugate base and increase the entropic penalty to the structure of water. Smaller alcohols and their conjugate bases are more soluble in water, with methoxide showing a greater solvation energy than tert-butoxide, for example. Consequently, in small alkanols, the solvation energy overcomes polarization effects, reversing, in solution, the acid-strength trend revealed for the gas phase.[20] The question is, *how does this dichotomy change at the gas-solid interface?*

Based on the two-state chemisorption equilibrium of alkanols on STO{100}, we define the *interfacial* Brønsted-Lowry acidity as: $(H\text{--}A)_{ads} \rightleftharpoons H^{+}_{ads} + A^{-}_{ads}$, where the hydrogen-bonded species serves as the "acid" ($(H\text{--}A)_{ads}$) that donates its proton to the surface as the hydrogen bond is broken, resulting in the broken-hydrogen-bond "conjugate base" species (A^{-}_{ads}). The interfacial acid (ia) dissociation constant, K_{ia}, is defined as the ratio of canonical partition functions of the products to the reactant (see Supplementary Section I.G.). A stronger acid has a greater K_{ia}, or lower pK_{ia} (= $-\log(K_{ia})$), and results from a lower free energy of the broken-hydrogen-bond species compared to the hydrogen-bonded-species.

The pK_{ia} values of the series of alkanols from methanol to butanol at 298 K, calculated using the experimentally observed "α-H close" or analogous orientation for each alkanol, are shown in Fig. 5. The optimized structures and adsorption energies for all alkanols are provided in Supplementary section I.E. The relationships between the structure of the alkanol and its pK_{ia} are revealed by a fit to the linear function: $pK_{ia} = Ax + By + C$, where x = number of carbon atoms in the alkanol, y = number of alkyl substituents on

the α carbon, A = -0.4701, B = 0.7363, and C = -0.7362 (*p* value of the χ^2 distribution of the fit = 0.997). While the gas-phase acidity of alcohols increases with *x* and *y* from methanol to butanol, and the corresponding aqueous acidity decreases with *x* and *y*, the interfacial acidity increases with *x* but decreases with *y*. On STO{100}, longer alkyl chains stabilize the conjugate base by enhancing van der Waals interactions between the base and the surface, resulting in a linear decrease in pK_{ia} with increase in *x* as chain lengths are increased at constant α-C substitution (red lines in Fig. 5, see Supplementary section I.F.). These interactions increase as the alkoxide approaches closer to the surface in the broken-hydrogen-bond form (O_{alk}-Ti = 1.91-1.93 Å in the broken-hydrogen-bond form compared to 1.95-1.96 Å in the hydrogen-bonded form across different alcohols). Furthermore, the strain in the O_{alk}-Ti-O_{surf} angle is released, changing from 78-79° in the hydrogen-bonded species to 86-88° as the O_{alk}-Ti bond is oriented more perpendicular to the surface in the broken-hydrogen-bond species. In contrast, greater alkyl substitution on the α-carbon compromises these alkyl-surface interactions in the broken-hydrogen-bond form and linearly increases pK_{ia} when the total number of carbons remains constant (green lines in Fig. 5), mainly by decreasing the number of α-hydrogen atoms that interact strongly with surface oxygen atoms. Since the magnitude of B is greater than that of A in the functional form of the pK_{ia} trend, increasing *x* and *y* each by one (i.e., increasing chain length and α-C substitution simultaneously) increases pK_{ia} (blue lines in Fig. 5), revealing the dominant role of substitution over chain length in interfacial acidity. Simply put, van der Waals interactions with the surface control interfacial acidity more than polarizability of the alkyl chain, similar to the way solvent interactions control aqueous acidity more than

polarizability effects. We note that variations in K_{ia} are dominated by changes in the ratio of electronic partition functions resulting from adsorption energies of the two chemisorbed forms for different alcohols (see Supplementary section I.G.). The adsorption energy of each chemisorbed form on STO{100} mirrors the trends of pK_{ia} such that adsorption energy increases with *x* but decreases with *y*, with the exception that sec-butanol adsorbs more strongly than n-butanol. Interfacial acid strength decreases with temperature, but the structural trends are preserved, as shown in Supplementary Figure S12.

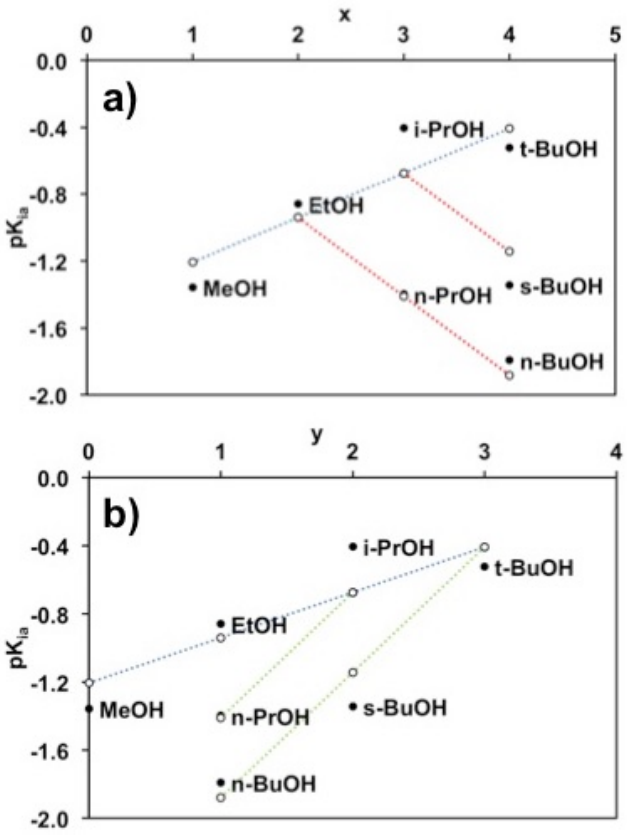

Fig. 5: pK_{ia} values for alkanols from methanol to butanol adsorbed on STO{100} at 298K. DFT-computed values (filled circles) and their fit to a linear function described in the text (open circles) are shown as a function of the total number of carbon atoms (*x*) in (a) and as a function of alkyl substituents on the α-carbon (*y*) in (b). Dotted lines are

provided to guide the eye through points in the fit. All structures and pK_{ia} values are provided in Supplementary Section I.G.

In summary, we combined DFT and SFG to determine the interfacial Brønsted-Lowry acidity of small alkanols adsorbed on STO{100}. Our work shows that the structure-acidity relationships of the alcohol are overall qualitatively different at the gas-oxide interface as compared to homogeneous gas and aqueous phases. The similarities with chain-length dependence in gas-phase acidity and alkyl-substituent dependence in aqueous acidity demonstrate that interfacial acidity produces a unique combination of contrary chemical trends observed in the two homogeneous phases. Our results show the critical role played by hydrogen bonding in controlling acidity and indicate its importance in acid-base transformations of alcohols on oxide surfaces at higher surface temperatures. The conceptualization of interfacial acidity is generalizable to other oxides, permitting a comparison of acidity of different molecules on a given surface, and, ultimately, broadening the description of a fundamentally important chemical property beyond homogeneous environments.

Computational Methods

DFT calculations were performed using the Perdew-Burke-Ernzerhof (PBE) exchange-correlation functional[25] and Grimme's D3 method of dispersion correction[26, 27] within the Vienna *ab initio* Simulation Package (VASP)[28-30] (Version 5.4.4). For all atoms, projector-augmented-wave potentials (PAW) were used to describe electron-core interactions.[31, 32] To allow for electron localization on the STO{100} surface, a Hubbard-

U correction of 11.0 eV was applied to the 3d orbitals of Ti atoms, using the approach introduced by Dudarev et al.[33] This correction was chosen as it resulted in a calculated band gap of 3.24 eV for bulk STO, similar to that found experimentally (3.25 eV).[34] An energy cutoff of 400 eV was used for the planewave basis set, and partial orbital occupancies were described using Gaussian smearing with a width of 0.05 eV. The bulk lattice constant was calculated to be 4.02 Å, in comparison to an experimental value of 3.91 Å.[35]

The TiO_2-terminated STO{100} surface was modeled by a 3 × 3 × 3 supercell with an additional layer of TiO_2 along the z-direction to allow for TiO_2 termination on both sides. A vacuum layer of 24 Å was added above the top surface layer. The total number of atoms in the supercell was 162, and adsorption of one isopropanol molecule created an adsorbate coverage of 1/9 ML. The Brillouin zone of the cell was sampled using a 3 × 3 × 1 Monkhorst-Pack k-point grid.[36] Geometry optimizations were performed using the quasi-Newton algorithm,[37] allowing the adsorbate species and the top surface layer (57 atoms) to relax until the force on each atom was less than 0.01 eV/Å. Transition states were calculated using the climbing-image nudged elastic band method.[38]

Experimental Methods

Sample preparation and characterization followed our previous work;[17] characterization results are shown in Supplementary section II. Similarly, a comprehensive description of the SFG spectrometer used in this experiment can be found elsewhere.[39, 40] Briefly, the output of a Spectra Physics Spitfire Pro Ti:Sapphire amplifier (output: <6 W, 1 kHz

repetition rate, ~45 fs pulses, centered near 800 nm) was split into two paths. The first path was directed into an optical parametric amplifier with difference-frequency mixer to generate broadband mid-infrared (IR) pulses tuned to excite the -OH stretching region. Approximately 2.4 W of the remaining laser output was directed into a pulse shaper to produce time-symmetric narrowband near-infrared (NIR) pulses[39, 40] used for up-conversion. The polarizations of both arms were purified using polarizers and subsequently rotated with waveplates before being collinearly combined with a dichroic optic. The beams were focused onto the STO{100} surface at an angle of 60° relative to the surface normal. An achromatic doublet collected the radiated SFG light before being polarization-resolved, filtered, spectrally resolved and detected. SFG spectra were background-subtracted and scaled by the nonresonant response obtained from the bare STO sample in the PPP polarization combination. The IR beam path and sample-environment enclosures were continuously purged with dry nitrogen to limit IR attenuation from atmospheric water.

The measured SFG intensity is proportional to the modulus-square of second-order nonlinear susceptibility, $\chi_{eff}^{(2)}$, and the incident driving laser fields, E_{IR} and E_{NIR}:

$$I_{SFG} \sim |\chi_{eff}^{(2)} E_{IR} E_{NIR}|^2. \quad (1)$$

The effective second-order nonlinear susceptibility, $\chi_{eff}^{(2)}$, is the sum of resonant and non-resonant, $\chi_{NR}^{(2)}$, contributions:

$$\chi_{eff}^{(2)} = \chi_{NR}^{(2)} + \sum_{q}^{n} \frac{A_q}{\omega_{IR} - \omega_q + i\Gamma_q} \quad (2)$$

where ω_{IR} is the frequency of incident IR laser light, ω_q is the resonance-transition frequency, A_q is the mode-specific amplitude, and Γ_q is the associated linewidth. Equation 2 shows that when the incident broadband IR light has spectral components that are resonant with molecular vibrations, there is an enhancement in the radiated signal. This enhancement serves to map the vibrational spectrum in an analogous way to conventional IR or Raman spectroscopies. Owing to the even-order field interaction (see Eq. 1), SFG is forbidden in isotropic and centrosymmetric bulk media.[41] Data was fit to Equations 1 and 2 and plotted in Figure 4 as solid lines.

Associated Content

A Supporting Information file containing computational results including STO surface stability, adsorption potential-energy-surface scan, alkanol adsorption structural and vibrational frequency data, extended discussions of van der Waals interactions and interfacial acidity is provided, along with experimental x-ray diffraction and atomic force microscopy surface characterization data. A separate file containing the atomic coordinates of all DFT-optimized structures reported in this work is also included.

Acknowledgment

Computations of the adsorption steps of isopropanol on STO{100} were supported by the UT-ORNL Joint Directed Research and Development (JDRD) Program of the Tennessee Science Alliance. Computations of the adsorption steps on other alkanols on STO{100} and calculations of interfacial acidity were supported by the National Science Foundation CAREER grant CHE-1753273. Computations were performed using

resources at the Center for Functional Nanomaterials, a U.S. DOE Office of Science Facility, and the Scientific Data and Computing Center, a component of the Computational Science Initiative, at Brookhaven National Laboratory under Contract No. DE-SC0012704. R.C.C. and S.R. also thank the Advanced Computing Facility and the National Institute of Computational Sciences at the University of Tennessee for ongoing computational resources and support. A.U.C. and B.D. were supported by the U.S. Department of Energy, Office of Science, Basic Energy Sciences, Chemical Sciences, Geosciences, and Biosciences Division. R.L.S was supported by the Department of Energy, Office of Science, Basic Energy Sciences, Materials Sciences and Engineering Division. S.R. thanks John E. Bartmess for discussions on alcohol acidity in gaseous and aqueous phases.

Author contributions

R.C.C., K.R.M., and S.R. performed the computational component of the research. A.U.C. and B.D. designed, carried out and analyzed SFG measurements. R.L.S. prepared and characterized the STO samples.

Competing interests

The authors declare no competing interests.

1. Das, S.; Imoto, S.; Sun, S.; Nagata, Y.; Backus, E. H. G.; Bonn, M., Nature of Excess Hydrated Proton at the Water–Air Interface. *Journal of the American Chemical Society* **2020,** *142* (2), 945-952.
2. Sengupta, S.; Moberg, D. R.; Paesani, F.; Tyrode, E., Neat Water–Vapor Interface: Proton Continuum and the Nonresonant Background. *The Journal of Physical Chemistry Letters* **2018,** *9* (23), 6744-6749.

3. Polo-Garzon, F.; Wu, Z., Acid–base catalysis over perovskites: a review. *Journal of Materials Chemistry A* **2018,** *6* (7), 2877-2894.
4. Sugunan, S.; Meera, V., Acid-base properties and catalytic activity of ABO3 (perovskite-type) oxides consisting of rare earth and 3d transition metals. *Reaction Kinetics and Catalysis Letters* **1997,** *62* (2), 327-332.
5. Foo, G. S.; Hood, Z. D.; Wu, Z., Shape Effect Undermined by Surface Reconstruction: Ethanol Dehydrogenation over Shape-Controlled SrTiO3 Nanocrystals. *ACS Catalysis* **2018,** *8* (1), 555-565.
6. Hammami, R.; Batis, H.; Minot, C., Combined experimental and theoretical investigation of the CO2 adsorption on LaMnO3+y perovskite oxide. *Surface Science* **2009,** *603* (20), 3057-3067.
7. Foo, G. S.; Polo-Garzon, F.; Fung, V.; Jiang, D.-e.; Overbury, S. H.; Wu, Z., Acid–Base Reactivity of Perovskite Catalysts Probed via Conversion of 2-Propanol over Titanates and Zirconates. *ACS Catalysis* **2017,** *7* (7), 4423-4434.
8. Rabuffetti, F. A.; Stair, P. C.; Poeppelmeier, K. R., Synthesis-Dependent Surface Acidity and Structure of SrTiO3 Nanoparticles. *The Journal of Physical Chemistry C* **2010,** *114* (25), 11056-11067.
9. Daturi, M.; Busca, G.; Willey, R. J., Surface and structure characterization of some perovskite-type powders to be used as combustion catalysts. *Chemistry of Materials* **1995,** *7* (11), 2115-2126.
10. Kuhn, J. N.; Ozkan, U. S., Surface properties of Sr- and Co-doped LaFeO3. *Journal of Catalysis* **2008,** *253* (1), 200-211.
11. Kubo, J.; Ueda, W., Catalytic behavior of AMoOx (A=Ba, Sr) in oxidation of 2-propanol. *Materials Research Bulletin* **2009,** *44* (4), 906-912.
12. Aramendía, M. A.; Borau, V.; Jiménez, C.; Marinas, J. M.; Porras, A.; Urbano, F. J., Magnesium Oxides as Basic Catalysts for Organic Processes: Study of the Dehydrogenation–Dehydration of 2-Propanol. *Journal of Catalysis* **1996,** *161* (2), 829-838.
13. Gervasini, A.; Auroux, A., Acidity and basicity of metal oxide surfaces II. Determination by catalytic decomposition of isopropanol. *Journal of Catalysis* **1991,** *131* (1), 190-198.
14. Rekoske, J. E.; Barteau, M. A., Kinetics and Selectivity of 2-Propanol Conversion on Oxidized Anatase TiO2. *Journal of Catalysis* **1997,** *165* (1), 57-72.
15. Trikalitis, P. N.; Pomonis, P. J., Catalytic activity and selectivity of perovskites La1−xSrxV1−x3+Vx4+O3 for the transformation of isopropanol. *Applied Catalysis A: General* **1995,** *131* (2), 309-322.
16. Varadarajan, T. K.; Sumathi, R.; Viswanathan, B., Partial oxidation of 2-propanol on perovskites. *Indian Journal of Chemistry -Section A* **2001,** *40A* (10), 1033-1036.
17. Tan, S.; Gray, M. B.; Kidder, M. K.; Cheng, Y.; Daemen, L. L.; Lee, D.; Lee, H. N.; Ma, Y.-Z.; Doughty, B.; Lutterman, D. A., Insight into the Selectivity of Isopropanol Conversion at Strontium Titanate (100) Surfaces: A Combination Kinetic and Spectroscopic Study. *ACS Catalysis* **2017,** *7* (12), 8118-8129.
18. Polo-Garzon, F.; Yang, S.-Z.; Fung, V.; Foo, G. S.; Bickel, E. E.; Chisholm, M. F.; Jiang, D.-e.; Wu, Z., Controlling Reaction Selectivity through the Surface Termination of Perovskite Catalysts. **2017,** *129* (33), 9952-9956.

19. Doughty, B.; Goverapet Srinivasan, S.; Bryantsev, V. S.; Lee, D.; Lee, H. N.; Ma, Y.-Z.; Lutterman, D. A., Absolute Molecular Orientation of Isopropanol at Ceria (100) Surfaces: Insight into Catalytic Selectivity from the Interfacial Structure. *The Journal of Physical Chemistry C* **2017,** *121* (26), 14137-14146.
20. Brauman, J. I.; Blair, L. K., Gas-phase acidities of alcohols. Effects of alkyl groups. *Journal of the American Chemical Society* **1968,** *90* (23), 6561-6562.
21. Brauman, J. I.; Blair, L. K., Gas-phase acidities of alcohols. *Journal of the American Chemical Society* **1970,** *92* (20), 5986-5992.
22. Bartmess, J. E.; Scott, J. A.; McIver, R. T., Scale of acidities in the gas phase from methanol to phenol. *Journal of the American Chemical Society* **1979,** *101* (20), 6046-6056.
23. Boand, G.; Houriet, R.; Gaumann, T., Gas-Phase Acidity of Aliphatic Alcohols. *Journal of the American Chemical Society* **1983,** *105* (8), 2203-2206.
24. Ghale, S. B.; Lanorio, J. G.; Nickel, A. A.; Ervin, K. M., Conformational Effects on Gas-Phase Acidities of Isomeric C3 and C5 Alkanols. *The Journal of Physical Chemistry A* **2018,** *122* (39), 7797-7807.
25. Perdew, J. P.; Burke, K.; Ernzerhof, M., Generalized Gradient Approximation Made Simple. *Physical Review Letters* **1996,** *77* (18), 3865-3868.
26. Grimme, S.; Antony, J.; Ehrlich, S.; Krieg, H., A consistent and accurate ab initio parametrization of density functional dispersion correction (DFT-D) for the 94 elements H-Pu. *The Journal of Chemical Physics* **2010,** *132* (15), 154104.
27. Grimme, S.; Ehrlich, S.; Goerigk, L., Effect of the damping function in dispersion corrected density functional theory. *Journal of computational chemistry* **2011,** *32* (7), 1456-1465.
28. Kresse, G.; Furthmüller, J., Efficiency of ab-initio total energy calculations for metals and semiconductors using a plane-wave basis set. *Computational Materials Science* **1996,** *6* (1), 15-50.
29. Kresse, G.; Hafner, J., Ab initio molecular dynamics for liquid metals. *Physical Review B* **1993,** *47* (1), 558-561.
30. Kresse, G.; Hafner, J., Ab initio molecular-dynamics simulation of the liquid-metal--amorphous-semiconductor transition in germanium. *Physical Review B* **1994,** *49* (20), 14251-14269.
31. Blöchl, P. E., Projector augmented-wave method. *Physical Review B* **1994,** *50* (24), 17953-17979.
32. Kresse, G.; Joubert, D., From ultrasoft pseudopotentials to the projector augmented-wave method. *Physical Review B* **1999,** *59* (3), 1758-1775.
33. Dudarev, S. L.; Botton, G. A.; Savrasov, S. Y.; Humphreys, C. J.; Sutton, A. P., Electron-energy-loss spectra and the structural stability of nickel oxide: An LSDA+U study. *Physical Review B* **1998,** *57* (3), 1505-1509.
34. Benthem, K. v.; Elsässer, C.; French, R. H., Bulk electronic structure of SrTiO3: Experiment and theory. *Journal of Applied Physics* **2001,** *90* (12), 6156-6164.
35. Maslen, E. N.; Spadaccini, N.; Ito, T.; Marumo, F.; Satow, Y., A synchrotron radiation study of strontium titanate. *Acta Crystallographica Section B* **1995,** *51* (6), 939-942.
36. Monkhorst, H. J.; Pack, J. D., Special points for Brillouin-zone integrations. *Physical Review B* **1976,** *13* (12), 5188-5192.

37. Pulay, P., Convergence acceleration of iterative sequences. the case of scf iteration. *Chemical Physics Letters* **1980,** *73* (2), 393-398.
38. Henkelman, G.; Uberuaga, B. P.; Jónsson, H., A climbing image nudged elastic band method for finding saddle points and minimum energy paths. *The Journal of Chemical Physics* **2000,** *113* (22), 9901-9904.
39. Chowdhury, A. U.; Liu, F.; Watson, B. R.; Ashkar, R.; Katsaras, J.; Patrick Collier, C.; Lutterman, D. A.; Ma, Y.-Z.; Calhoun, T. R.; Doughty, B., Flexible approach to vibrational sum-frequency generation using shaped near-infrared light. *Opt. Lett.* **2018,** *43* (9), 2038-2041.
40. Chowdhury, A. U.; Watson, B. R.; Ma, Y.-Z.; Sacci, R. L.; Lutterman, D. A.; Calhoun, T. R.; Doughty, B., A new approach to vibrational sum frequency generation spectroscopy using near infrared pulse shaping. *Review of Scientific Instruments* **2019,** *90* (3), 033106.
41. Wang, H.-F.; Velarde, L.; Gan, W.; Fu, L., Quantitative Sum-Frequency Generation Vibrational Spectroscopy of Molecular Surfaces and Interfaces: Lineshape, Polarization, and Orientation. *Annual Review of Physical Chemistry* **2015,** *66* (1), 189-216.